

**Fractal space-scale unfolding mechanism for energy-efficient turbulent mixing**S. Laizet<sup>\*</sup> and J. C. Vassilicos<sup>†</sup>*Turbulence, Mixing and Flow Control Group, Department of Aeronautics, South Kensington, Imperial College, London SW7 2BZ, United Kingdom<sup>‡</sup>*

(Received 1 May 2012; published 1 October 2012)

Using top-end high fidelity computer simulations we demonstrate the existence of a mechanism present in turbulent flows generated by multiscale or fractal objects and which has its origin in the multiscale or fractal space-scale structure of such turbulent flow generators. As a result of this space-scale unfolding mechanism, fractal grids can enhance scalar transfer and turbulent diffusion by one order of magnitude while at the same time reduce pressure drop by half. This mechanism must be playing a decisive role in environmental, atmospheric, ocean, and river transport processes wherever turbulence originates from multiscale or fractal objects such as trees, forests, mountains, rocky riverbeds, and coral reefs. It also ushers in the concept of fractal design of turbulence which may hold the power of setting entirely new mixing and cooling industrial standards.

DOI: [10.1103/PhysRevE.86.046302](https://doi.org/10.1103/PhysRevE.86.046302)

PACS number(s): 47.27.wj, 47.27.E–

Nature is replete with multiscale or fractal objects, such as trees, forests, mountains, coral reefs, rough ocean surfaces, and irregular sea and riverbeds which interact with air or water flow and create turbulence. The question arises whether the turbulent flows thus generated can transport and mix heat, moisture, biological, chemical and/or polluting substances and perhaps also propagate fires faster and/or more efficiently than turbulent flows conventionally studied in the laboratory.

This fundamental question has also direct applied physics implications. Static obstacles of various shapes, called mixing elements by the industries involved, are routinely placed inside industrial static inline mixers or exhaust ducts in order to reorient the flow in various alternate directions and/or create turbulence so as to achieve mixing [1]. The nuclear and process industries routinely use so-called spacer grids and rod baffles to achieve enhanced heat transfer and cooling in cylindrical geometries such as shell-and-tube heat exchangers [2]. Is there an advantage in copying nature and designing fractal spacer grids and baffles as well as fractal mixing elements for static inline mixers?

Fractal geometry has been a mathematical and, in science, a mostly descriptive activity [3,4] till the late 1980s and 1990s when research on the linear physics of fractals started [5,6]. Studies of turbulent flows with fractal or multiscale inlet boundary conditions have only recently been emerging [7–10]. In this paper we report on the stirring and transport properties of turbulent flows generated by fractal objects.

A good setting for such a study is grid-generated turbulent flow [11–13] in a wind tunnel or water channel. In such a setting, the grid is placed at and covers the entry of a tunnel or channel test section and the flow moves through the grid towards the test section and along it. As the flow moves through the grid it becomes turbulent. This turbulence determines both the pressure drop across the grid and the random stirring which can cause transfers, turbulent diffusion and, thereby, mixing.

In this computational study we calculate and compare the effects of fractal and regular grids on scalar transfer

and turbulent diffusion efficiencies [14–16]. As a result we report a mechanism which greatly increases scalar transfer and turbulent diffusion and at the same time reduces pressure drop and therefore power losses. We carry out this study in a generic configuration which can just about be reached by current top-end high performance computing and massive numerical code parallelization. It is possible, of course, to study more specific configurations in the laboratory, but it is extremely hard, if not impossible, to obtain full flow and pressure field information from laboratory measurements in the way that our numerical computations allow us to do. These entire flow and pressure fields provide a wealth of information which enables us to draw simple conclusions and understanding such as the space-scale unfolding (SSU) mechanism which has potential for broad applicability in the natural and applied sciences.

We consider two grids, one regular and one fractal [see Fig. 1(a)] of same blockage ratio  $\sigma = 0.507$  (ratio of the area blocked by the grid to the area  $T^2$  of the channel or tunnel square section), same thickness in the streamwise direction (normal to the grid), and same effective mesh size  $M_{\text{eff}} = \frac{4T^2}{L_G} \sqrt{1 - \sigma}$  where  $L_G$  is the total length of the grid when it has been stripped of its thickness [7]. The concept of an effective mesh size was defined and introduced by [7]; in the case of regular grids,  $M_{\text{eff}}$  equals  $M$ , the actual mesh size [see Fig. 1(a)].

Each grid is placed in a computational domain with streamwise length  $L_x$  and spanwise extents  $L_y = L_z = T$ . For the fractal grid,  $L_x = 1152t_{\text{min}}$  and  $T = 144t_{\text{min}}$  where  $t_{\text{min}}$  is the spanwise thickness of the smallest bars on the grid [see Fig. 1(a)]. For the regular grid,  $L_x = 576b$  and  $T = 36b$  where  $b$  is the spanwise thickness of the bars on the grid [see Fig. 1(a)]. The streamwise thickness of both grids is  $3t_{\text{min}}$  and the boundary layers are laminar at the grid resulting in boundary layer thicknesses smaller than  $0.5t_{\text{min}}$ ; also  $b = 2t_{\text{min}}$  and  $M_{\text{eff}} = 6.5t_{\text{min}}$ .

We assume a fluid of uniform density and kinematic viscosity  $\nu$  and inflow-outflow boundary conditions in the streamwise direction with a uniform fluid velocity  $U_\infty$  without turbulence as inflow condition and a one-dimensional (1D) convection equation as outflow condition. The boundary conditions in the two spanwise directions are periodic. Defining  $\mathbf{x} \equiv (x, y, z)$  to be spatial coordinates in the streamwise ( $x$ ) and two spanwise directions, the inflow is at  $x = -14M_{\text{eff}}$

<sup>\*</sup>s.laizet@imperial.ac.uk<sup>†</sup>j.c.vassilicos@imperial.ac.uk<sup>‡</sup>www.imperial.ac.uk/tmfc

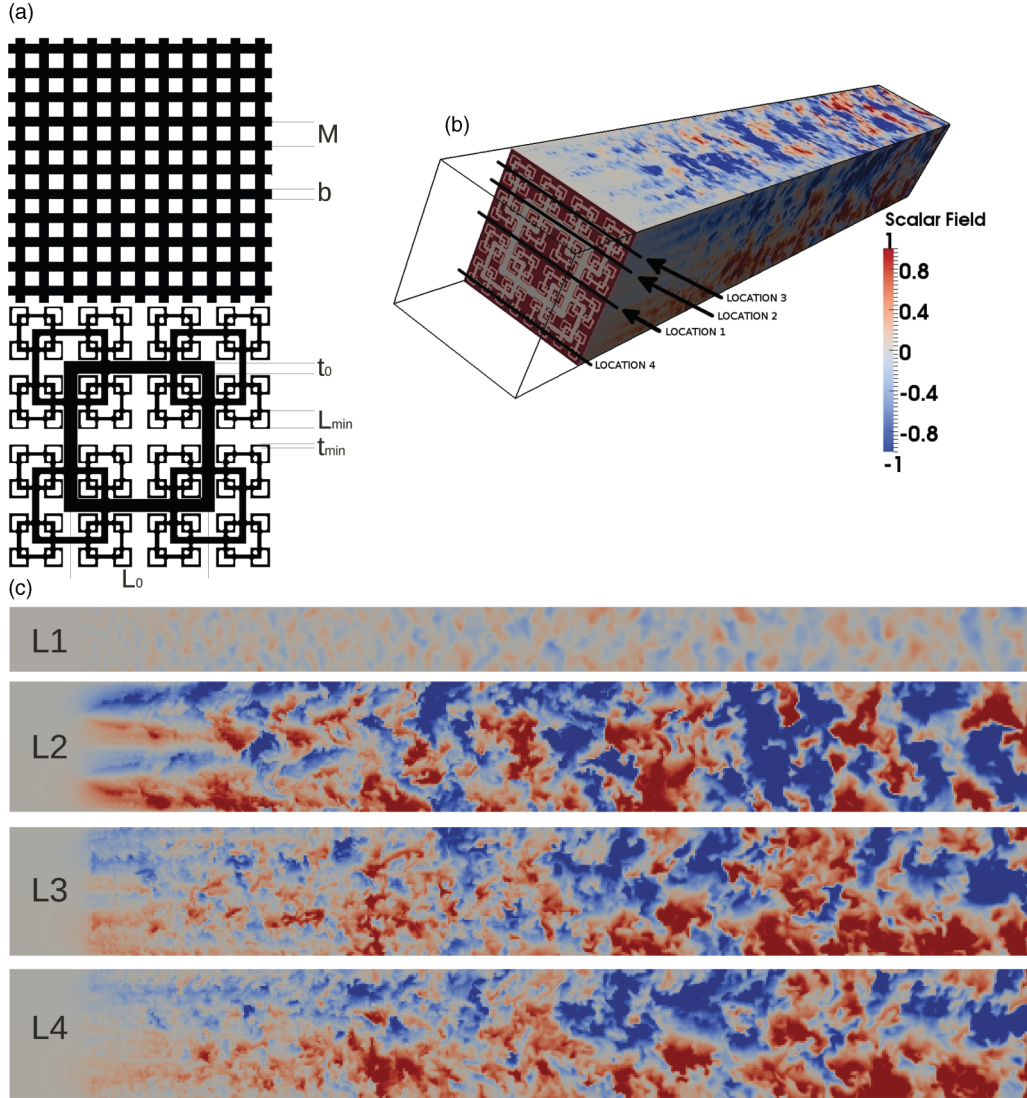


FIG. 1. (Color online) (a) Regular (mesh size  $M$  and bar thickness  $b$ ) and fractal monoplanar grids of same  $\sigma$ ,  $M_{\text{eff}}$ , and streamwise thickness. Four iterations of bar lengths  $L_n = 2^{-n}T/2$  ( $L_{\text{min}} = L_3$ ) and thicknesses  $t_n = (2.041)^{3-n}t_{\text{min}}$ ,  $n = 0, 1, 2, 3$  on the fractal grid. (b) 3D visualization of computational domain with grid and downstream scalar field  $\theta$ . (c) 2D  $(x, y)$  cuts through the scalar field  $\theta$ . Top is for regular grid. Then locations 1,2,3 are for fractal grid where different size wakes are visible.

and the grid is placed at  $x = 0$ . The inlet Reynolds number  $\text{Re} \equiv \frac{U_\infty M_{\text{eff}}}{\nu}$  is 1950 for both grid cases. Our initial condition for the velocity field is  $\mathbf{u} \equiv (u, v, w) = (U_\infty, 0, 0)$  everywhere [ $u$  is the streamwise velocity component and  $(v, w)$  are the two spanwise velocity components corresponding to  $(y, z)$ ].

In the code Incompact3D, which we use to solve on a Cartesian mesh the incompressible Navier-Stokes and the scalar transport equations, the grids are modeled by the immersed boundary method following a procedure proposed by [17]. In terms of the Kolmogorov microscale  $\eta$  (the smallest length scale of the turbulence), the spatial resolution is at worse  $\Delta x = \Delta y = \Delta z \leq 4\eta$  for the fractal grid and  $\leq 8\eta$  for the regular grid (where the turbulence is at its most intense, i.e., in 5% of the computational domain, with  $\eta \approx 0.125t_{\text{min}}$  for the fractal grid and  $\approx 0.0625t_{\text{min}}$  for the regular grid) and  $\Delta x = \Delta y = \Delta z \leq 2\eta$  for the remaining 95% of the computational domain for both grids (at the end of the

computational domain,  $\eta \approx 0.375t_{\text{min}}$  for the fractal grid and  $\approx 0.286t_{\text{min}}$  for the regular grid). The time step is  $0.01t_{\text{min}}/U_\infty$  and resolves our flows' smallest time scales which are  $\eta/U_\infty$ . Full details about the code, its validations, and its application to grid-generated turbulence can be found in Refs. [18,19]. For the fractal grid flow the Cartesian mesh has 2881 mesh nodes in the streamwise direction and  $360 \times 360$  mesh nodes in the other two directions, i.e., about 374 million mesh nodes in total, and is split in 8100 computational cores. For the regular grid flow, the Cartesian mesh has 2881 mesh nodes in the streamwise direction but  $180 \times 180$  mesh nodes in the other two directions, i.e., about 93 million mesh nodes in total, and is split in 7200 computational cores. The size of the present simulations are such that we have no alternative but to use the parallel version of this code [20]. We ran it on HECToR's Cray XE6 system (based on six-core processors; HECToR is the UK's national supercomputing facility).

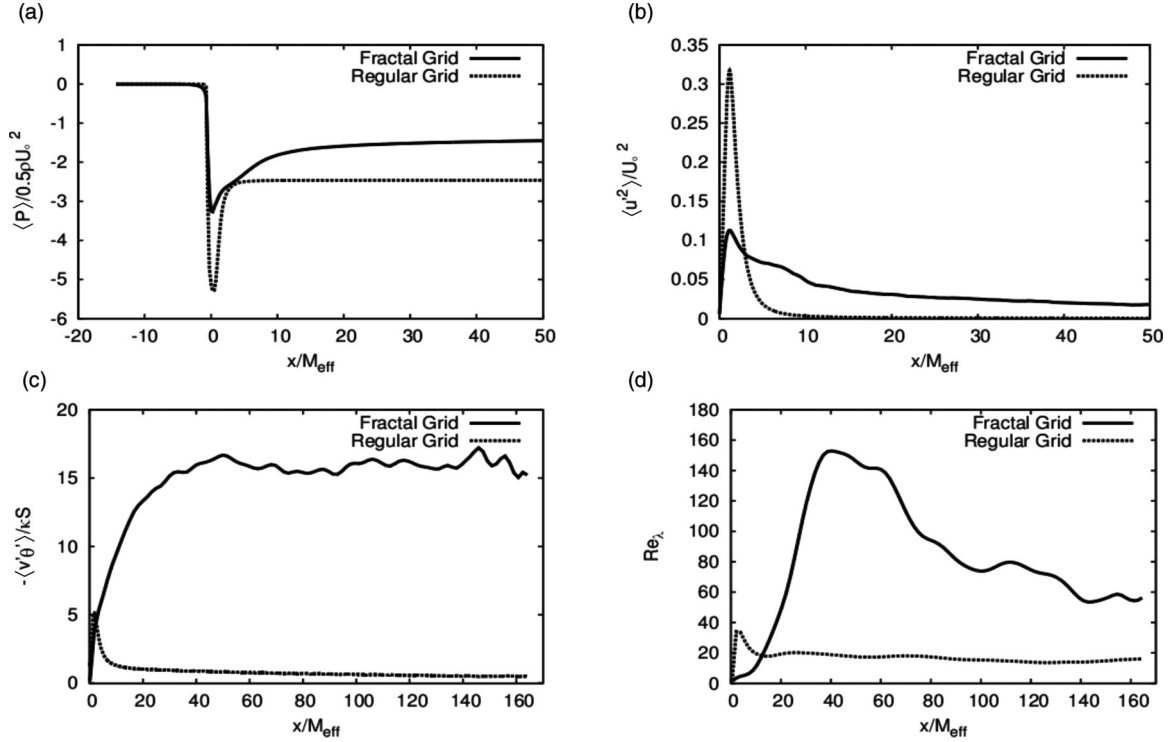


FIG. 2. (a) Normalized average pressure, (b) average square turbulence intensity, and (c) normalized transverse turbulent scalar transfer. Averages are over  $y, z$  and time. (d) Center line  $Re_\lambda$ . All plots show dependencies on streamwise coordinate normalized by the effective mesh size  $M_{\text{eff}}$ .

The scalar field  $\theta(\mathbf{x}, t)$  is advected by the velocity field and diffused by molecular processes, i.e., our code solves

$$\frac{\partial \theta}{\partial t} + \mathbf{u} \cdot \nabla \theta = \kappa \nabla^2 \theta, \quad (1)$$

with molecular diffusivity  $\kappa = 10\nu$ . The initial condition we impose on this scalar field is  $\theta(\mathbf{x}, 0) = Sy$  where  $S$  is a constant scalar gradient and the inflow condition is  $\theta = Sy$  at all times. The other boundary conditions for  $\theta$  are outflow in the streamwise end of the computational domain, periodic in the  $z$  direction and Neumann in the  $y$  direction. These conditions are the simplest way to initiate and sustain a turbulent scalar flux [15,21,22]. The fact that  $S$  is independent of position in space simplifies comparisons between grids as there is no distribution of length scales inherent to the initial scalar field to take into account. Figure 1 includes 2D cuts through 3D scalar fields for the regular and the fractal grids. The scalar is dimensionless and  $St_{\text{min}} = 1/16$  for both grid cases.

The first statistics we extract from our data are  $\langle P \rangle$  and  $\langle \mathbf{u} \rangle$  where  $P$  is the pressure divided by the fluid's mass density and the brackets signify an average over  $y, z$  and time. We find  $\langle \mathbf{u} \rangle = (U_\infty, 0, 0)$  at all  $x$  for both grids and we plot  $2\langle P \rangle / U_\infty^2$  versus  $x/M_{\text{eff}}$  in Fig. 2(a). In that same figure we also plot [Fig. 2(b)] the square turbulence intensity  $\langle u'^2 \rangle / U_\infty^2$  versus  $x/M_{\text{eff}}$ , where  $u' \equiv u - \bar{u}$  and the overline signifies an average over time only. For both grids,  $\langle P \rangle$  peaks immediately downstream of the grid. It is perhaps remarkable that  $\langle u'^2 \rangle / U_\infty^2$  peaks at about one  $M_{\text{eff}}$  from both grids. Even though  $M_{\text{eff}}$  was introduced by [7], this is a compelling demonstration of the relevance of this geometrically defined effective mesh size to

grid-generated turbulence. Plots such as those in Figs. 2(a) and 2(b) are virtually impossible to obtain experimentally as they require full field measurements of both pressure and velocity fields.

Also noteworthy in Figs. 2(a) and 2(b) are the differences between the fractal and the regular grids. The regular grid generates a much higher peak average turbulence intensity and a much higher peak average pressure drop than the fractal grid, which is consistent. However, the fractal grid returns a much longer pressure recovery length and, consistent with this, a much slower average turbulence decay. The fractal grid's average turbulence intensity is significantly larger than the regular grid's from about  $5M_{\text{eff}}$  from the grid till the end of our computational domain at  $163M_{\text{eff}}$ . The average normalized pressure drop between upstream and far downstream of the fractal grid is about half that of the regular grid [see Fig. 2(a)] even though their blockage ratio is the same.

For both grids, the transverse turbulent transfer of scalar fluctuations  $\theta' \equiv \theta - \bar{\theta}$  in the direction of the initial scalar gradient does not vanish [see Fig. 2(c) where we plot  $\langle \theta' v' \rangle / (\kappa S)$ ], whereas we find that  $\langle \theta' u' \rangle = \langle \theta' w' \rangle = 0$  ( $v' \equiv v - \bar{v}$ ,  $w' \equiv w - \bar{w}$ ). This transverse scalar transfer peaks at a distance equal to about  $1.6M_{\text{eff}}$  from the regular grid but at about  $47M_{\text{eff}}$  from the fractal grid, in which case it also saturates beyond  $47M_{\text{eff}}$ . Beyond  $47M_{\text{eff}}$  and up till the end of our computational domain, the transverse scalar transfer is between 19 to 32 times larger for the fractal grid than for the regular grid; specifically, the ratio of  $\langle \theta' v' \rangle$  for the fractal grid to  $\langle \theta' v' \rangle$  for the regular grid is equal to about 19 at a distance  $47M_{\text{eff}}$  from the grid and 32 at the end of our computational domain.

Along the center line  $y = z = T/2$ , the time-averaged  $\overline{\theta'v'}$  behaves very much like  $\langle\theta'v'\rangle$  for both grids. Along that center line, the local Taylor length-scale Reynolds number  $Re_\lambda \equiv \sqrt{u'^2}\lambda/\nu$  [the Taylor length scale  $\lambda$  is defined by  $\lambda^2 \equiv u'^2/(\frac{\partial u'}{\partial x})^2$ ] peaks for both grids at the distance from the grid where the transverse scalar transfer peaks [see Fig. 2(d)]. The streamwise location of this peak requires another length scale, different from  $M_{\text{eff}}$ , to be explained, namely the wake-interaction length scale  $x_*$  introduced by [8].

On the fractal grid, neighboring bars of the smallest spanwise thickness  $t_3 = t_{\min}$  are separated by a length  $L_3$  so that the wakes from these neighboring bars meet at a distance from the grid which scales as  $L_3^2/t_3$  because the two wakes grow with  $x$  as  $y_w \sim \sqrt{t_3 x}$  and they meet where  $y_w = L_3$  [8]. One can expect increased turbulence activity where this interaction happens. The wakes from neighboring bars of spanwise thickness  $t_2$  meet at a distance from the grid which scales as  $L_2^2/t_2$  and  $L_2^2/t_2 > L_3^2/t_3$ . The same can be said about wakes from bars of spanwise thickness  $t_1$  and also about the largest bars of spanwise thickness  $t_0$  thus leading to four successive length scales:  $L_3^2/t_3 \approx 12.5M_{\text{eff}} < L_2^2/t_2 \approx 24.5M_{\text{eff}} < L_1^2/t_1 \approx 48M_{\text{eff}} < L_0^2/t_0 \approx 94M_{\text{eff}}$  [see schematic in Fig. 3(a)]. The largest is the wake-interaction length scale  $x_* = L_0^2/t_0$ : it characterizes the distance from the grid where all wakes have met other wakes and, in particular, another wake of their own size. For the regular grid, the wake interaction length scale is  $x_* = M^2/b = 3.26M = 3.26M_{\text{eff}}$  because all wakes have the same single size.

Plots of the transverse scalar transfer  $\langle\theta'v'\rangle$  and  $Re_\lambda$  as functions of  $x/x_*$  [see Figs. 3(c) and 3(d)] show quite clearly that both the scalar transfer and  $Re_\lambda$  peak at around  $\frac{1}{2}x_*$  for both grids. This observation agrees with wind tunnel measurements of  $u'^2$  and  $Re_\lambda$  along the centerline [8,13,23] and demonstrates that the streamwise location of the peak in  $\langle\theta'v'\rangle$  and  $Re_\lambda$  occurs where all wakes have finally interacted with other same-size wakes. The streamwise locations where successive same-size wakes meet seem to be approximately  $\frac{1}{2}L_3^2/t_3 \approx 6.25M_{\text{eff}} < \frac{1}{2}L_2^2/t_2 \approx 12.25M_{\text{eff}} < \frac{1}{2}L_1^2/t_1 \approx 24M_{\text{eff}} < \frac{1}{2}L_0^2/t_0 \approx 47M_{\text{eff}}$ .

The existence of successive distances from the grid where different same-size pairs of wakes meet is the essence of the space-scale unfolding (SSU) mechanism. This mechanism is absent from regular grid turbulence where all wakes meet their neighboring wakes at the same short distance from the grid causing a great burst of intense turbulence very near the grid and a fast decay of this turbulence within less than one  $x_* = M^2/b$ . As a result, the pressure drop is very steep downstream of a regular grid and the pressure recovery fast (see Fig. 2), in fact within about half an  $x_*$ , which is only  $1.6M$  in this case.

The presence of the SSU mechanism when turbulence is generated by fractal grids such as Fig. 1(b) means that, for the same blockage ratio, the spatial distribution of length scales on the fractal grid unfolds onto the streamwise extent of the flow and gives rise to a variety of wake-meeting distances downstream. As a result, the grid's turbulence generation is distributed in the streamwise direction causing the turbulence

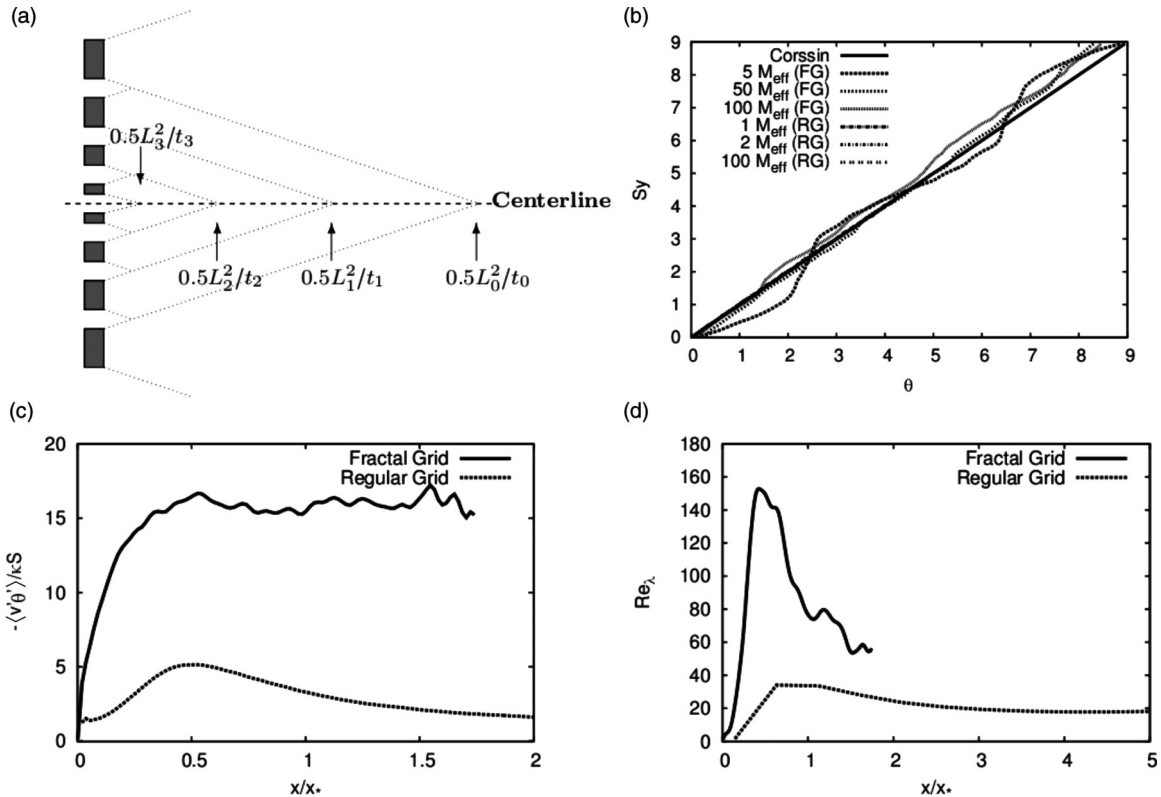


FIG. 3. (a) Schematic behind the SSU mechanism. (b)  $\bar{\theta}$  at  $z = 0$  fluctuates around  $\theta(x,0) = Sy$  (line marked  $t = 0$ ). Different curves for different  $x$  positions and both grids. Similar results are obtained at other  $z$  positions. (c) Normalized transverse turbulent scalar transfer averaged over  $y, z$  and time and (d) center line  $Re_\lambda$  as functions of streamwise coordinate normalized by the wake-interaction length scale  $x_*$ .

to be less and the pressure drop smaller very near the grid by comparison to a same blockage regular grid, but also causing a much longer pressure recovery and a much slower turbulence decay in multiples of  $M_{\text{eff}}$ . In multiples of  $x_*$ , however, the pressure recovery and turbulence decay distances remain of the order of  $x_*$  as in the regular grid case, but  $x_*/M_{\text{eff}}$  is one order of magnitude larger for the fractal grid.

The SSU mechanism can also explain the scalar transfer enhancement caused by the fractal grid. We find for both grids that  $\bar{\theta} \approx Sy + \theta_r$ , where  $\theta_r$  is a randomly fluctuating variable around a constant [see Fig. 3(b); this is a non-trivial result reminiscent of one by [21] for homogeneous isotropic turbulence, see also [24]]. In our computations, advection dominates over molecular diffusion in Eq. (1), and we can therefore write  $\theta(\mathbf{x}_0, 0) \approx \theta(\mathbf{x}, t)$  where  $\mathbf{x} = \mathbf{x}_0 + \int_0^t \mathbf{u}(\mathbf{x}(\tau), \tau) d\tau$ . It follows that  $\theta'(\mathbf{x}, t) \approx Sy_0 - Sy - \theta_r$  and therefore  $\overline{\theta'v'} \approx -S(y - y_0)v'$  where  $\overline{(y - y_0)v'}$  is a turbulent diffusivity.

From a Lagrangian viewpoint, therefore, one can see how the SSU mechanism can increase turbulent diffusivity and thereby scalar transfer. Imagine a fluid element starting off near the grid at a  $y = y_0$  in one of the smallest wakes. In the case of the regular grid, this fluid element will travel inside this wake and perhaps meet another wake of the same size and its  $y$  coordinate will therefore predominantly remain close to  $y_0$ . However, in the case of the fractal grid, the fluid element will have a chance of jumping into a larger wake as it travels downstream, and then an even larger one again, each time encountering a turbulence with a larger

eddy turnover length scale. As a result,  $y - y_0$  will be much larger than for the regular grid for many fluid elements and so will turbulent diffusion and scalar transfer. The SSU mechanism also distributes turbulent eddy length scales along the streamwise direction, in increasing size from near the grid to about  $\frac{1}{2}x_*$  at which point all wake pairs of all sizes have met. This is also the region where the scalar transfer increases, and it remains constant and larger than the scalar transfer of the regular grid by an order of magnitude beyond that point. Note that the argument in this and the previous paragraphs requires high Peclet number in order to write  $\overline{\theta'v'} \approx -S(y - y_0)v'$  and high Reynolds number for the wakes to be turbulent but makes no assumption on the Schmidt or Prandtl number.

The SSU mechanism has its root cause in the multiscale space-scale structure of the fractal grid and therefore may be expected to be present with more or less effect in a wide range of turbulent flows originating from trees, forests, mountains, coral reefs, rough sea or riverbeds, and coastlines all of which have their own multiscale or fractal structure. The SSU mechanism may, for example, play a crucial role in the fast propagation of forest fires. We have shown that this mechanism can cause enhancements of scalar transfer and turbulent diffusion of at least one order of magnitude as well as very significant reductions in pressure drop and power losses. Applying this mechanism to energy-efficient industrial mixers and heat transfer devices has the potential to set entirely new mixing and cooling standards.

We acknowledge EPSRC Grant No. EP/H030875/1.

- 
- [1] S. Hirschberg, R. Koubek, F. Moser, and J. Schock, *Chem. Eng. Res. Design* **87**, 524 (2009).
  - [2] G. F. Hewitt, *Heat Exchanger Design Handbook* (Begell House, New York, 1998).
  - [3] B. Mandelbrot, *The Fractal Geometry of Nature* (W. H. Freeman & Co., San Francisco, 1982).
  - [4] K. J. Falconer, *Fractal Geometry: Mathematical Foundations and Applications* (John Wiley, Chichester, 1990).
  - [5] M. V. Berry, *Physica D* **38**, 29 (1989).
  - [6] B. Sapoval and T. Gobron, *Phys. Rev. E* **47**, 3013 (1993).
  - [7] D. Hurst and J. C. Vassilicos, *Phys. Fluids* **19**, 035103 (2007).
  - [8] N. Mazellier and J. C. Vassilicos, *Phys. Fluids* **22**, 075101 (2010).
  - [9] K. Nagata, H. Suzuki, H. Sakai, Y. Hayase, and T. Kubo, *Phys. Scr.*, T **132**, 014054 (2008).
  - [10] F. Nicolleau, S. Salim, and A. Nowakowski, *J. Turbulence* **12**(44), 1 (2011) [<http://www.tandfonline.com/doi/abs/10.1080/14685248.2011.637046>].
  - [11] G. I. Taylor, *Proc. R. Soc. A* **151**, 421 (1935).
  - [12] G. Comte-Bellot and S. Corrsin, *J. Fluid Mech.* **48**, 273 (1971).
  - [13] Jayesh and Z. Warhaft, *Phys. Fluids* **4**, 2292 (1992).
  - [14] B. I. Shraiman and E. D. Siggia, *Nature (London)* **6787**, 639 (2000).
  - [15] Z. Warhaft, *Annu. Rev. Fluid Mech.* **32**, 203 (2000).
  - [16] H. Suzuki, K. Nagata, H. Sakai, and R. Ukai, *Phys. Scr.*, T **142**, 014069 (2010).
  - [17] P. Parnaudeau, J. Carlier, D. Heitz, and E. Lamballais, *Phys. Fluids* **20**, 085101 (2008).
  - [18] S. Laizet and E. Lamballais, *J. Comput. Phys.* **228**, 5989 (2009).
  - [19] S. Laizet and J. C. Vassilicos, *Flow Turbul. Combust.* **87**, 673 (2011).
  - [20] S. Laizet and N. Li, *Int. J. Numer. Methods Fluids* **67**, 1735 (2011).
  - [21] S. Corrsin, *J. Appl. Phys.* **33**, 113 (1952).
  - [22] H. K. Wiskind, *J. Geophys. Res.* **67**, 30 (1962).
  - [23] P. Valente and J. C. Vassilicos, *J. Fluid Mech.* **687**, 300 (2011).
  - [24] L. Mydlarski and Z. Warhaft, *J. Fluid Mech.* **358**, 135 (1998).